Bringing physics to life at the submesoscale

Marina Lévy, Ramiro Ferrari, Peter J. S. Franks, Adrian P. Martin, Pascal Rivière

Bringing physics to life at the submesoscale

Marina Lévy,[1] Raffaele Ferrari,[2] Peter J. S. Franks,[3] Adrian P. Martin,[4] and Pascal Rivière[5]

Received 15 June 2012; accepted 19 June 2012; published 27 July 2012.

[1] A common dynamical paradigm is that turbulence in the upper ocean is dominated by three classes of motion: mesoscale geostrophic eddies, internal waves and microscale three-dimensional turbulence. Close to the ocean surface, however, a fourth class of turbulent motion is important: submesoscale frontal dynamics. These have a horizontal scale of O(1–10) km, a vertical scale of O(100) m, and a time scale of O(1) day. Here we review the physical-chemical-biological dynamics of submesoscale features, and discuss strategies for sampling them. Submesoscale fronts arise dynamically through nonlinear instabilities of the mesoscale currents. They are ephemeral, lasting only a few days after they are formed. Strong submesoscale vertical velocities can drive episodic nutrient pulses to the euphotic zone, and subduct organic carbon into the ocean's interior. The reduction of vertical mixing at submesoscale fronts can locally increase the mean time that photosynthetic organisms spend in the well-lit euphotic layer and promote primary production. Horizontal stirring can create intense patchiness in planktonic species. Submesoscale dynamics therefore can change not only primary and export production, but also the structure and the functioning of the planktonic ecosystem. Because of their short time and space scales, sampling of submesoscale features requires new technologies and approaches. This paper presents a critical overview of current knowledge to focus attention and hopefully interest on the pressing scientific questions concerning these dynamics.
Citation: Lévy, M., R. Ferrari, P. J. S. Franks, A. P. Martin, and P. Rivière (2012), Bringing physics to life at the submesoscale, *Geophys. Res. Lett.*, *39*, L14602, doi:10.1029/2012GL052756.

1. Introduction

[2] The ocean's storage of carbon and ability to regulate atmospheric carbon dioxide is crucially dependent on primary production, the creation of organic matter from inorganic nutrients and carbon through photosynthesis. The transport of limiting nutrients to the sunlit surface ocean (the euphotic zone) plays a central role in controlling primary production. It has been argued that turbulent eddy motions are an important vehicle for this transport [*Falkowski et al.*, 1991; *Flierl and Davis*, 1993; *Oschlies and Garcon*, 1998; *Mahadevan and Archer*, 2000; *Martin and Richards*, 2001; *Lévy et al.*, 2001; *Williams and Follows*, 2003]. Although the subject of some debate [*Oschlies*, 2002; *McGillicuddy et al.*, 2003; *Martin and Pondaven*, 2003] it has been claimed that in some regions of the ocean as much as half of the nitrate supply may be driven by eddy-induced vertical motions [*McGillicuddy et al.*, 1998]. The other essential ingredient for photosynthesis is light. Turbulent motions modulate the availability of light by moving phytoplankton through the euphotic zone [*Sverdrup*, 1953; *Lévy et al.*, 1998; *Taylor and Ferrari*, 2011a]. The nutrient and light environments that regulate global primary production, the export of fixed carbon to depth and ultimately the efficiency of the ocean's biological carbon storage, are thus intimately intertwined with these turbulent motions.

[3] Until a few years ago, the dynamical paradigm was that turbulence in the upper ocean is dominated by three classes of motion: mesoscale geostrophic eddies, internal waves and microscale three-dimensional turbulence. Geostrophic eddies are generated through barotropic and baroclinic instabilities of the mean currents at mesoscales of O(10–100) km and dominate the eddy kinetic energy of the ocean. The mesoscale eddies twist and fold tracer filaments resulting in a cascade of tracer variance to smaller scales, while they interact and pair resulting in a cascade of energy to larger scales. Internal waves, generated by surface winds and tidal forcing at scales O(0.1–10) km, interact and drive a transfer of energy toward smaller spatial scales. Microscale turbulence at scales O(0.01) km and less arises from three-dimensional instabilities driven by air-sea fluxes in the turbulent boundary layers and from breaking internal gravity waves in the interior. The absence of an energy cascade to smaller scales separates mesoscale turbulence from internal waves and microscale turbulence that transfer energy to molecular dissipation scales.

[4] There is a rich literature on the impact of these three phenomena on biological dynamics in the ocean. Geostrophic eddies can regulate both the lateral [e.g., *Williams and Follows*, 1998; *Oschlies*, 2002; *Lévy*, 2003; *Ferrari et al.*, 2008; *Lehahn et al.*, 2011; *Chelton et al.*, 2011] and vertical [e.g., *McGillicuddy et al.*, 1998; *Uz et al.*, 2001; *Cipollini et al.*, 2001; *Martin and Richards*, 2001; *McGillicuddy et al.*, 2007] transport of biomass and nutrients. Internal waves affect production by periodically heaving biomass into the euphotic zone [e.g., *Holloway and Denman*, 1989]. Microscale turbulence maintains well-mixed biomass and nutrients within the turbulent surface boundary layer as well as driving nutrient fluxes into the mixed layer [e.g., *Lewis et al.*, 1986] and particulate and dissolved organic carbon out of it [e.g., *Ruiz et al.*, 2004].

[5] Recent observations and numerical simulations, however, suggest that close to the ocean surface a fourth class of turbulent motion is important: submesoscale frontal dynamics [e.g., *Thomas et al.*, 2008; *Ferrari*, 2011]. Submesoscale

[1]LOCEAN, IPSL, CNRS/UPMC/IRD/MNHN, Paris, France.
[2]Department of Earth, Atmospheric and Planetary Sciences, Massachusetts Institute of Technology, Cambridge, Massachusetts, USA.
[3]Scripps Institution of Oceanography, University of California, San Diego, La Jolla, California, USA.
[4]National Oceanography Centre, Southampton, UK.
[5]LEMAR, IUEM, CNRS/IRD/UBO, Plouzané, France.

Corresponding author: M. Lévy, LOCEAN, IPSL, CNRS/UPMC/IRD/MNHN, BC100, 4, place Jussieu, F-75252 Paris CEDEX 05, France. (marina@locean-ipsl.upmc.fr)

0094-8276/12/2012GL052756

fronts arise at scales just smaller than the mesoscale: a horizontal scale of O(1–10) km, i.e., less than the first baroclinic deformation radius; a vertical scale of O(100) m, i.e., thinner than the main thermocline; and a time scale of O(1) day. Submesoscale fronts arise dynamically through advective interactions involving mesoscale currents (and thus are distinct from inertial-gravity waves on comparable spatial scales). They are, importantly, influenced by Earth's rotation and by density stratification (unlike microscale turbulence). Most importantly, submesoscale fronts are distinct from the filaments generated by mesoscale stirring, because they are characterized by density jumps and sharp velocity jets. Mesoscale stirring is inefficient at transferring potential (density filaments) and kinetic (narrow jets) energy to scales below the first deformation radius. Frontogenesis at the ocean surface (and other boundaries) breaks this constraint and results in a transfer of energy from the mesoscale to fronts and then all the way to dissipation through secondary frontal instabilities, as we discuss below. From the perspective of this review, the emergence of submesoscale fronts is particularly important because they can regulate the exchange of properties between the turbulent boundary layer and the ocean interior.

[6] The relative contribution of the various turbulent motions to the evolution of a tracer is best illustrated in terms of the Reynolds-averaged equation – the equation describing the dynamics of the long-time average of the tracer. For illustrative purposes, let us consider the concentration of nutrient N averaged over a time/spatial scale larger than the mesoscale field. The average evolves according to:

$$\partial_t \overline{N} + \underbrace{\overline{u}.\nabla\overline{N}}_{mean} = \underbrace{-\nabla_H \cdot \overline{u'N'}}_{mesoscale} - \underbrace{\partial_z \overline{w'N'}}_{submesoscale} + \underbrace{\partial_z\left(\overline{k_z \partial_z N}\right)}_{microscale} + \underbrace{\overline{B(N)}}_{biology} \quad (1)$$

where overbars indicate averages and primes denote eddy fluctuations over this spatio-temporal scale. For clarity, we have separated the microscale Reynolds fluxes, which are associated with irreversible mixing of water masses, and the mesoscale and submesoscale Reynolds fluxes, which represent advective transport of material properties along density surfaces without irreversible mixing. The horizontal advective Reynolds fluxes are dominated by mesoscale eddies [*Ledwell et al.*, 1998]. The vertical advective Reynolds fluxes are dominated by mesoscale eddies in the ocean interior away from boundaries, but there is growing evidence that in the upper few hundred meters of the oceans they are dominated by submesoscale circulations at fronts [e.g., *Capet et al.*, 2008; *Klein and Lapeyre*, 2009]; evidence of the more active role of submesoscales in the vertical Reynolds flux is presented in section 3.3. The effect of microscale turbulence often referred to as vertical mixing, is particularly strong in the turbulent boundary layers, where it keeps tracers and momentum well mixed. In this equation it is parameterized as a vertical diffusivity term, with k_z the vertical diffusion coefficient. Finally, *B(N)* denotes all biological processes affecting the concentration of *N*. Typically, for nitrate *B(N)* includes uptake by phytoplankton and production through nitrification. An equation similar to Equation (1) holds for phytoplankton, except that the "biology" term accounts for phytoplankton growth minus losses such as death and respiration.

[7] The potential role of the submesoscale has only recently been recognized; thus, compared to the other terms in the above equation little is known about its magnitude, distribution and contribution to vertical and horizontal fluxes. This paper presents a critical overview of current knowledge to focus attention and hopefully interest on the pressing scientific questions concerning these dynamics.

[8] The paper is organized into 6 parts. Section 2 reviews the main characteristics of submesoscale dynamics. Section 3 examines how these dynamics are likely to affect the nutrient and phytoplankton budget of the euphotic layer. Section 4 focuses on the impact of submesoscale dynamics on the structure and spatial distributions of the planktonic ecosystem. Section 5 discusses the observational difficulties associated with investigating submesoscale heterogeneities. Finally, section 6 comprises the Conclusions.

2. Submesoscale Dynamics

[9] Stirring by large-scale ocean currents and mesoscale eddies creates a convoluted web of filaments of all oceanic tracers, including temperature, salinity, nutrients and phytoplankton. However, only close to the ocean surface does the filamentation of hydrographic properties evolve into sharp density fronts with associated strong submesoscale circulations (Figure 1). The theory of frontogenesis at the ocean surface is well understood and the interested reader is referred to the many excellent in-depth reviews [e.g., *Hoskins*, 1982; *Thomas et al.*, 2008; *Klein and Lapeyre*, 2009]. Here we offer a heuristic argument to explain why submesoscale fronts are generated preferentially at the ocean surface. Note that fronts can also be generated at the ocean bottom, but our focus is on the impact of fronts on ocean productivity in the upper ocean.

[10] At the mesoscale, i.e., scales larger than the first deformation radius of O(10–100) km [*Chelton et al.*, 1998], the pressure gradients associated with horizontal density fronts are balanced by the Coriolis acceleration due to Earth's rotation: the so-called "geostrophic balance". The degree of geostrophic balance is quantified in terms of the Rossby number $Ro = U/fL$, where U is the characteristic velocity at a front, L is the frontal width and f is the Coriolis parameter: geostrophic balance holds if $Ro \ll 1$. In the ocean interior, density surfaces are very flat with a steepness smaller than $O(Ro)$. Whenever the mesoscale or large-scale velocity field is locally convergent and acts to compress and steepen density surfaces, an overturning circulation develops that promptly brings the surfaces back toward the horizontal (reducing their steepness) and restores the geostrophic balance (increasing L). Hence submesoscale motions with $Ro = O(1)$ do not arise spontaneously in the ocean's interior. A convergent velocity field, however, compresses passive tracers that have no feedback on the dynamics. Indeed mesoscale turbulence in the ocean interior continuously generates sharp tracer filaments, a process referred to as a forward cascade of enstrophy and tracer variance [*Charney*, 1971]. It is only density surfaces that remain smooth [*Lapeyre et al.*, 2006; *Klein et al.*, 2008].

[11] The situation is quite different at the ocean surface. In regions of flow convergence where density surfaces are brought together, the overturning circulation, that in the interior slumps surfaces back to the horizontal, becomes purely horizontal at the surface because water cannot cross

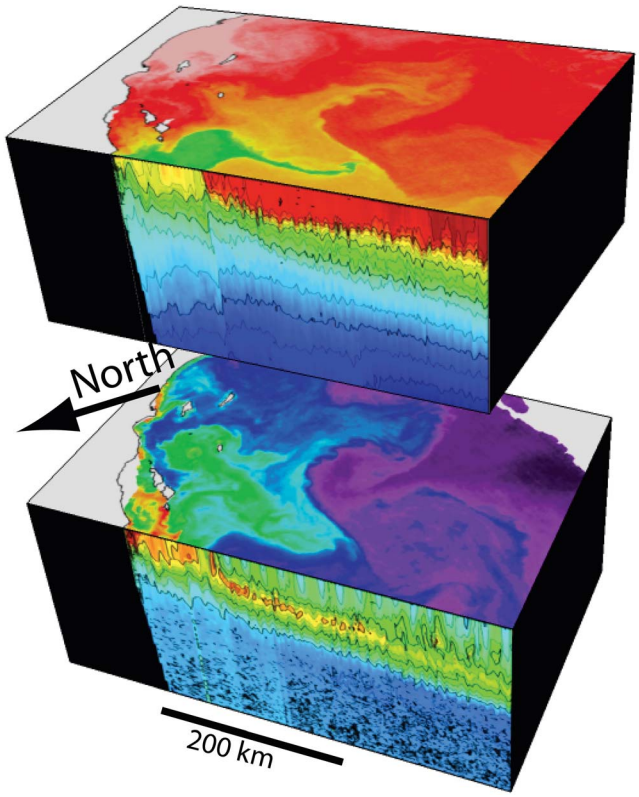

Figure 1. Three-dimensional views looking southeastward from Point Conception (California, USA) showing MODIS satellite remote sensing data combined with *in situ* glider data (www.sccoos.org/data/spray/). (top) Temperature. (bottom) Chlorophyll *a*. Ocean temperature is a good proxy for density in this part of the ocean. The surface mesoscale patterns seen in the temperature and chlorophyll *a* can also be seen as subsurface fluctuations in the isopycnal surfaces. The strong fronts and eddies are sites of strong submesoscale dynamics which can drive local responses of the phytoplankton.

the air-sea interface. The horizontal circulation acts to further accelerate the convergence of density surfaces resulting in frontogenesis – the formation of sharp density fronts in a time of a few days [*Hoskins and Bretherton*, 1972; *Spall*, 1995]. As the fronts form, the slope of the density surfaces increases (the slope is further increased by microstructure turbulence in the surface mixed layer which mixes away any vertical stratification) and *Ro* becomes O(1). The increase in *Ro* results in strong ageostrophic submesoscale circulations that drive a forward energy cascade and excite local microstructure turbulence [*Molemaker et al.*, 2010; *Taylor and Ferrari*, 2010]. The increase in slope is accompanied by the development of intense upwelling and downwelling on the warm and cold sides of the front respectively: the ratio of vertical to horizontal velocities scales with the slope of density surfaces and it is therefore much larger at fronts. In the ocean interior, with frontal aspect ratios of $O(10^{-4} - 10^{-3})$ and horizontal velocities of O(0.1) m/s, the vertical velocities reach $O(10^{-5} - 10^{-4})$ m s^{-1} or O(1–10) m d^{-1}. Near the surface the vertical velocities reach $O(10^{-3})$ m s^{-1} or O(100) m d^{-1} [*Mahadevan and Tandon*, 2006; *Legal and Tréguier*, 2007; *Klein and Lapeyre*, 2009]. These large vertical velocities extend from just below the surface down to a few hundred meters and drive a rapid exchange of properties between the turbulent boundary layer and the permanent thermocline (Figure 2a).

[12] Submesoscale fronts are ephemeral and typically last only a few days after they are formed. This is either because the flow convergence ceases as currents and mesoscale eddies evolve, or because the fronts become unstable. During frontolysis (frontal decay) the vertical velocity and the associated exchange of properties with the ocean interior progressively decrease. The shutdown is particularly rapid and extreme when frontolysis is associated with frontal instabilities [*Boccaletti et al.*, 2007; *Capet et al.*, 2008; *Thomas and Ferrari*, 2008], sometimes taking just a few hours. There is a rapidly growing literature on the details of how such instabilities develop. In the first stage, light waters flow over dense waters in what is called symmetric instability, a process that has recently been observed at the Kuroshio [*D'Asaro et al.*, 2011] and Gulf Stream fronts [*Thomas and Joyce*, 2010]. Later, meanders and eddies develop along the front and slumping accelerates as a result of baroclinic instability [*Fox-Kemper et al.*, 2008]. Other forms of instability have also been reported when the lateral shear at the front is particularly intense [*McWilliams*, 2010]. Regardless of the details of specific processes, the instabilities typically result in restratification and suppression of vertical mixing within the turbulent boundary layer (i.e., a strong decrease of k_z in equation (1)).

[13] *Thomas* [2005] points out that frontolysis can be arrested by winds. If the winds blow in the same direction as the frontal current, they act to steepen the front and prevent further slumping by frontal instabilities. In such situations turbulent mixing is enhanced at fronts, rather than being reduced, and no restratification takes place [e.g., *Franks and Walstad*, 1997]. If the winds blow in the opposite direction of the frontal current they act to slump the front, further accelerating restratification by frontal instabilities.

[14] In summary, one expects frontogenesis whenever large-scale currents or mesoscale eddies converge to bring together different water masses. During this phase strong vertical velocities develop which promote exchange of properties between the surface ocean and the permanent thermocline. Once the convergent flow weakens, frontolysis effectively suppresses turbulent mixing at the front except when winds blow in the direction of the frontal current.

3. Response of Phytoplankton to Submesoscale Dynamics

[15] The response of phytoplankton to submesoscale dynamics will typically depend on what factor exerts the main control over phytoplankton growth, light or nutrients. In case of nutrient limitation, the contribution of the submesoscale is mostly through the supply of nutrients into the nutrient starved euphotic layer. However, some of the most productive regions are in the high latitudes, where spring blooms are light limited. In the case of light limitation, the impact of submesoscales is mostly to modulate the strength of vertical mixing and thus the light exposure of phytoplankton. Moreover, in both cases, submesoscale processes will export phytoplankton out of the surface layer. These mechanisms, how they combine and their potential impact on large scale fluxes, are presented in this section.

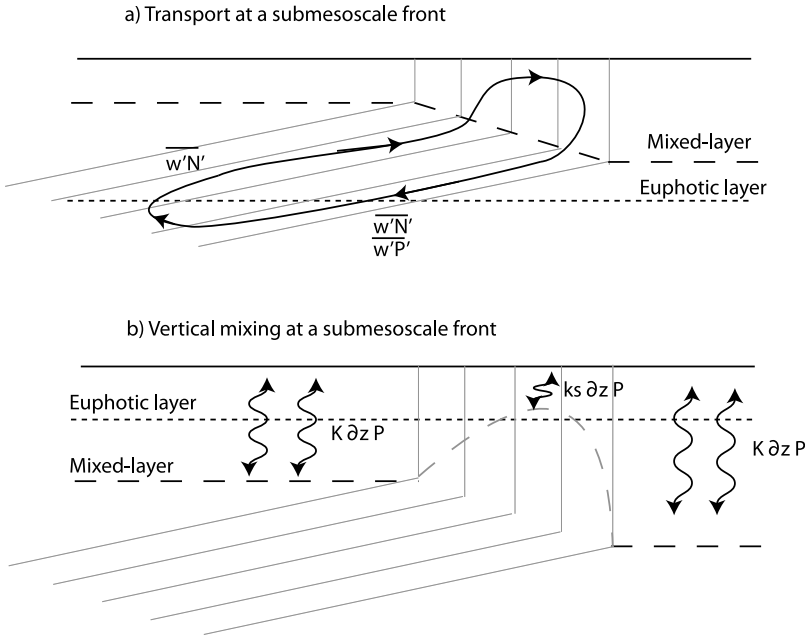

Figure 2. Schematic representation of how submesoscale advection and diffusion impacts biogeochemistry. (a) Advection: the upwelling branch of the ageostrophic circulation at a submesoscale front provides nutrient to the euphotic layer while the downwelling branch exports excess nutrient and organic material below the euphotic layer, along isopycnals. These processes prevail in situations where primary production is controlled by the availability of nutrients; in such cases the mixed-layer is shallower than the euphotic depth. (b) Vertical mixing: the reduction of vertical diffusivity at a mesoscale front is illustrated here as a reduction in the mixed-layer depth and in vertical mixing coefficient (K > ks); this process prevails when primary production is inhibited by strong vertical diffusivity, which causes phytoplankton to be mixed in and out of the euphotic layer; at the front, this mixing is reduced and phytoplankters remain in the well lit euphotic zone, which favors their growth with respect to out of front areas.

3.1. Response to Submesoscale Vertical Transport

[16] Over much of the ocean, phytoplankton growth is constrained by the availability of nutrients, which are abundant beneath the euphotic zone. The upward component of the submesoscale vertical circulation enhances the nutrient flux into the euphotic layer, stimulating phytoplankton growth (Figure 2a) [*Mahadevan and Archer*, 2000; *Lévy et al.*, 2001; *Allen et al.*, 2005; *Lapeyre and Klein*, 2006; *Nagai et al.*, 2008; *Johnson et al.*, 2010; *Pidcock et al.*, 2010]. Submesoscale upwelling can also drive deep phytoplankton biomass upward, alleviating light limitation of growth [*Lévy et al.*, 2001]. The downward branch, however, has a negative impact on primary production by subducting phytoplankton, together with other organic matter, out of the euphotic zone (Figure 2a) [*Kadko et al.*, 1991; *Fielding et al.*, 2001; *Lévy et al.*, 2001; *Niewiadomska et al.*, 2008; *Thomas and Joyce*, 2010]. This subduction acts as a physical carbon pump and modifies the properties of intermediate mode waters [*Karleskind et al.*, 2011a, 2011b]. Submesoscale vertical motions will occur in all regions, not just those that are nutrient limited. Purely from a perspective of vertical transport, therefore, the net biogeochemical effect of submesoscale dynamics may vary with region, representing a changing balance of the two antagonistic effects [*Lathuilière et al.*, 2010]. The strength of the submesoscale vertical advection also varies in space and time depending in part on the intensity of the eddy activity, and can be enhanced by winds through the generation of inertial motions [*Franks and Walstad*, 1997] that interact with the submesoscale frontogenetic dynamics [*Lévy et al.*, 2009].

[17] Much of our knowledge on this topic comes from models. For example, simulations suggest that submesoscale turbulence increases phytoplankton abundance in the open ocean [*Lévy et al.*, 2001; *Oschlies*, 2002; *McGillicuddy et al.*, 2003] but decreases it in eastern boundary upwelling regions [*Lathuilière et al.*, 2011]. Some studies also suggest that in regions where nutrients are plentiful, such as the subpolar North Atlantic or eastern boundary upwelling systems, submesoscale vertical circulations could cause a loss of nutrients from the euphotic layer [*Lévy et al.*, 2000; *Oschlies*, 2002; *McGillicuddy et al.*, 2003; *Gruber et al.*, 2011]. More generally, the regional net flux of nutrients due to submesoscale vertical advection depends on the often strongly localized distribution of enhanced vertical circulation and the rate of removal of upwelled nutrients from the upwelling regions by horizontal advection [*Martin et al.*, 2002; *Martin*, 2003; *Pasquero et al.*, 2005]. Typically, capturing the full strength of submesoscale vertical movements requires horizontal model resolution of the order of one tenth of the internal Rossby radius of deformation. This would require a resolution of O(1) km at mid-latitudes, though this depends on the mixed-layer depth. Studies with a coarser resolution will not fully capture the vertical circulation.

[18] There are only a few observational studies to complement these model results: the balance between upwelling and subduction of nutrients, phytoplankton and other organic material is inherently difficult to assess purely from

observations, let alone quantifying how this balance varies with the intensity of submesoscale turbulence. The magnitude of submesoscale turbulence can be evaluated from mean properties such as eddy kinetic energy or descriptors such as the Lyapunov exponent of the flow. This approach to quantifying the link between the vertical transport of nutrients and the strength of the submesoscale flow was applied by *Rossi et al.* [2008] and *Gruber et al.* [2011] in eastern boundary upwelling regions and by *Calil and Richards* [2010] in the oligotrophic open ocean. These studies report a positive correlation between productivity and eddy kinetic energy derived from altimetry in the open ocean, but the opposite relationship for eastern boundary upwelling regions. Although it is too early to discern any clear pattern, these results are at least consistent with the modelling studies described earlier.

[19] Submesoscale upwelling of nutrients to the surface also depends on how deep the submesoscale vertical velocities extend into the water column. The strength of the submesoscale vertical circulation is typically maximal at the base of the mixed layer. In situations of nutrient limitation, the largest vertical gradient of dissolved nutrients, the nutricline, is found at the base of the euphotic layer. The mixed layer is often shallower than the nutricline. In this case submesoscale upwelling will not be effective in mixing nutrients into the euphotic zone. A few studies have suggested that significant submesoscale vertical velocities can, in some circumstances, penetrate deeper than the mixed layer, potentially reaching the nutricline [*Capet et al.*, 2008; *Lévy et al.*, 2010]. In contrast to the submesoscale, the mesoscale vertical circulation is maximal at the zero crossing of the first baroclinic mode, which is often found deeper in the water column (∼500–1000 m).

[20] The time scales associated with upwelling will also determine its influence on primary production: the delivery of nutrients by mesoscale eddies may be more efficient than submesoscale motions for biological growth [*McGillicuddy et al.*, 2007]. Though the vertical velocities associated with mesoscale eddies are much smaller than the submesoscale ones due to the different *Ro* of the two regimes, the residence time of nutrients in the euphotic layer is longer for mesoscale eddies than for submesoscale fronts, potentially allowing for more complete uptake of the upwelled nutrients. Submesoscale fronts bring nutrients so rapidly in and out of the euphotic layer that it is unclear whether phytoplankton can fully utilize them. Indeed, typically, the time scale of nutrient supply at the surface by submesoscale vertical velocities is of the order of 0(1–10) day, which corresponds to the time scale of nutrient uptake by phytoplankton. Our current — rather incomplete — view of how the relationship between submesoscale and mesoscale vertical velocities varies with depth and time is a topic that clearly requires further research.

[21] Finally, in terms of carbon, how the air-sea CO_2 exchange is affected by submesoscale vertical transport is not straightforward. For instance, there are compensating effects of the small-scale upwelling of nutrients and cold temperatures, which tend to decrease oceanic pCO_2, and the upwelling of dissolved inorganic carbon (DIC), which tends to increase it [*Mahadevan et al.*, 2004, 2011]. The leading term of this balance depends on the relative vertical gradients of DIC (and alkalinity), nitrate and temperature. In the Northeast Atlantic, large submesoscale surface pCO_2 gradients have been observed, but attributed to stirring by mesoscale eddies rather than to vertical advection associated with submesoscale circulations [*Resplandy et al.*, 2009].

3.2. Response to Reduced Vertical Mixing at Submesoscale Fronts

[22] When light is the main factor limiting phytoplankton production, such as in large parts of the Southern Ocean or at high latitudes prior to the spring bloom, the reduction of vertical mixing induced by submesoscale dynamics can locally increase the mean time that photosynthetic organisms spend in the well-lit euphotic layer and promote primary production. This can be rationalized by the reduction of k_z in Equation 1, with the consequence of limiting phytoplankton excursions out of the euphotic layer (Figure 2b). Models suggest that this reduction of vertical mixing can either result in a reduction in the mixed-layer depth [*Lévy et al.*, 1998] or in a reduction of mixing intensity within the mixed-layer [*Taylor and Ferrari*, 2011a, 2011b]. This may lead to the beginning of a bloom prior to seasonal stratification, and has been reported in the North Atlantic by *Townsend et al.* [1994] and *Joyce et al.* [2009], as well as in the Adriatic by *Santoleri et al.* [2003]. Model studies of this phenomenon in the Mediterranean Sea [*Lévy et al.*, 1999, 2000] suggest that it only modifies the annual mean budget of phytoplankton production in the absence of strong seasonality. Otherwise, the main effect seems to be restricted to the earlier onset of the bloom [*Lévy et al.*, 2005; *Taylor and Ferrari*, 2011a, 2011b]. The importance of this process over large-scale, light-limited regions (such as in the Southern Ocean) remains to be assessed.

3.3. Response to Large-Scale Changes of the Circulation Induced by Submesoscale Dynamics

[23] The effects on nutrients of local mesoscale and submesoscale perturbations of the velocities do not cancel out when averaged over a regional scale. This is due to the nonlinear nature of advection. Mathematically, this local effect is associated with the Reynolds terms (see Equation 1). However, a complete picture of the impact of submesoscale turbulence on nutrients has to account not only for the local Reynolds fluxes but also for how the distribution of the large-scale circulation and nutrient fields (and hence the mean advection and vertical diffusion) are modified by submesoscale phenomena. For instance, the feedback of the submesoscale motions on the mean circulation may influence the position and strength of western boundary currents, and through the thermal wind balance, the global equilibration of the thermocline and nutricline [*Lévy et al.*, 2010]. In this sense there is an effect that is non-local in space and time, and can be thought of as the remote effect of the submesoscale dynamics. To demonstrate this impact it is necessary to run model experiments long enough to allow the model mean state to equilibrate in the presence of submesoscale dynamics. Clearly there is a practical issue of the computational demands associated with this. One example, however, is provided by the model study of *Lévy et al.* [2012]. Here, phytoplankton abundance at equilibrium was found to be less in the submesoscale-resolving (1/54°) model than in the model without submesoscale processes. This result arises from the different large-scale distributions of the nutricline depth and mixed-layer depth in the two model equilibria.

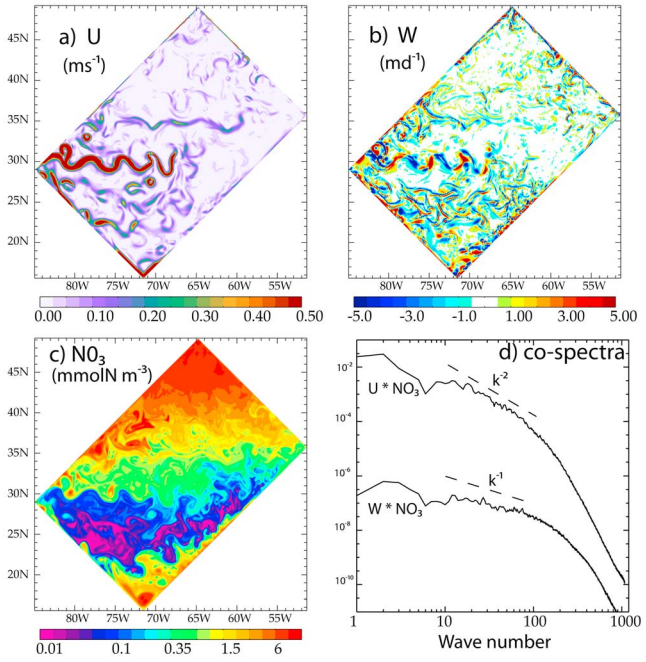

Figure 3. Snapshots of (a) modulus of horizontal velocity (U), (b) vertical velocity (W) and (c) nitrate concentration (NO_3, in log scale) from an idealized submesoscale-resolving model simulation representative of the Northwest Atlantic or Northwest Pacific subtropical to subpolar regions. Model fields are shown at 50 m depth, in winter (Dec 1st). (d) Co-spectra of U * NO_3 and W* NO_3, plotted in log-log scale.

[24] An attempt to quantify the contribution of submesoscales to the annual nitrate balance in the euphotic layer at mid-latitudes is presented here in the context of the *Lévy et al.* [2012] model. A seasonally varying double-gyre is simulated, representative of an idealized sector of the Northwest Atlantic or Pacific. A strong surface jet, the model's equivalent of the Gulf Stream or Kuroshio, flows eastward at ~30°N (Figure 3a). The instability of this jet generates intense mesoscale turbulence which is maximum in the vicinity of the jet but can be found throughout the region 20–40°N. The submesoscale circulation can be seen in the form of submesoscale jets (Figure 3a), accompanied by intense upwellings and downwellings on either side of the jets (Figure 3b). The nutrient concentration at the surface is characterized by a large-scale gradient, characteristic of the North Atlantic, and distorted by mesoscale stirring (Figure 3c). The long model spin-up (50 years) allows the annual mean position of the jet, as well as the thermocline and nutricline depths to reach equilibrium, integrating the feedback of submesoscale processes on large-scale quantities.

[25] The model domain is large enough to encompass different biological regimes: an oligotrophic regime in the subtropical gyre (from ~20–30°N) where winter nitrate concentrations are less (Figure 3c), a strong spring bloom in the subpolar gyre north of ~40°N and a mid-latitude regime with a moderate bloom between 30–40°N in the inter-gyre region. This north–south gradient in productivity is reflected by the structure of the biological term $B(N)$ (Figure 4).

[26] At equilibrium, an annual integration of all the terms in equation (1) implies that $\partial_t N$ is zero and thus the biological term $B(N)$ is exactly balanced by the sum of the four physical terms. After integration over the euphotic depth, this leads to:

$$\int_{1year}\int_{z=0}^{Zeupho}\left[-\underbrace{\overline{u}.\nabla\overline{N}}_{remote}-\underbrace{\nabla_H\cdot\overline{u'N'}}_{mesoscale(local)}-\underbrace{\partial_z\overline{w'N'}}_{submesoscale(local)}+\underbrace{\partial_z\left(k_z\partial_z\overline{N}\right)}_{remote}\right]dzdt=\int_{1year}\int_{z=0}^{Zeupho}\underbrace{\overline{B(N)}}_{biology}dzdt. \quad (2)$$

[27] The remote effect of submesoscales enters this equation through the mean advection and the vertical mixing terms. This is because submesoscale dynamics influence the mean currents, the mixed-layer depth and the mean distribution of nutrients. The local effects enter the equation through the horizontal and vertical Reynolds fluxes. Here, the separation between mean and eddy fields was done with a space filter with a cut-off scale of O(100) km. Thus the Reynolds terms potentially contain the contribution of both the mesoscale and the submesoscale. However, spectra of horizontal and vertical nitrate flux vs. wavenumber k show that the horizontal flux spectrum (slope of $\sim k^{-2}$) is steeper than the vertical flux spectrum (slope of $\sim k^{-1}$) and implies that the integral over wavenumbers is dominated by the largest scales (small wavenumbers) in the case of the horizontal flux, but it is strongly affected by the smallest scales (large wave numbers) in the case of the vertical flux. The overall vertical tracer flux is thus strongly affected by the submesoscale fronts.

[28] The contribution of the different terms in Equation 2 to the annual balance of nutrient supply to the euphotic layer varies regionally (Figure 4), as does the relative importance of the local (Reynolds) and remote (mean) submesoscale contributions. Vertical mixing dominates the balance in the regions where the mixed layer gets deeper than the euphotic depth over the seasonal cycle. This is the case north of 40°N and in the eastern sector. In these regions the local submesoscale term is negligible. In contrast, in the intergyre region (30–40°N), the mean and mesoscale advection terms are larger than vertical mixing and tend to oppose each other. In this region the local submesoscale term has a magnitude comparable to the other advective terms and is always positive. Thus, in this region local submesoscale advection is efficiently supplying nitrate to the euphotic layer; this supply makes a substantial contribution to the overall balance.

4. Ecosystem Response to Submesoscale Dynamics

[29] All the submesoscale dynamics described previously have the potential to change not only the primary and export production, but also the structure and the functioning of the planktonic ecosystem. Strong submesoscale vertical velocities can drive episodic nutrient pulses into the euphotic zone, while horizontal stirring can create intense patchiness in planktonic species. These processes have been investigated with both models and data.

[30] Many field studies have observed systematic changes in phytoplankton community structure across trophic gradients: the fraction of total biomass contributed by the smallest cells decreases strongly with increasing biomass

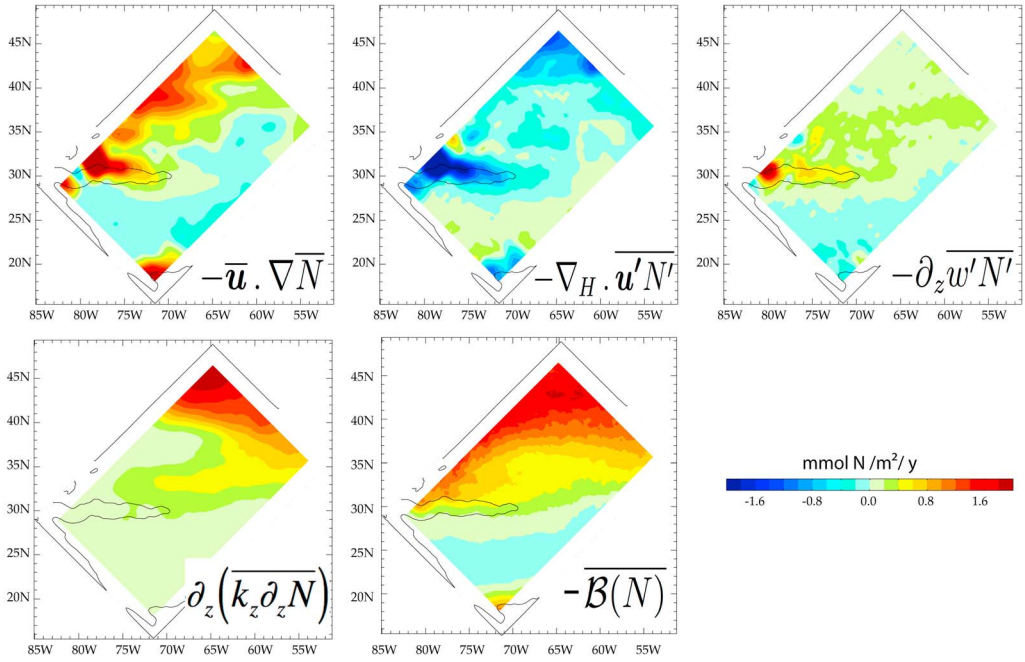

Figure 4. Contribution of all terms in the nitrate ($N = NO_3$) equation (equation (1)) from an idealized model simulation representative of the Northwest Atlantic or Northwest Pacific subtropical to subpolar regions. The terms are averaged over the year and over the euphotic depth, as in equation (2). The model is at equilibrium, hence the biological term $\int_{1year}\int_{z=0}^{Zeupho}\overline{B(N)}dzdt$ is exactly balanced by the sum of the four physical terms $\int_{1year}\int_{z=0}^{Zeupho}\left[-\overline{u}.\nabla\overline{N}-\nabla_H\cdot\overline{u'N'}-\partial_z\overline{w'N'}+\partial_z\left(\overline{k_z\partial_z N}\right)\right]dzdt$. The black contour shows the annual mean location of the model's idealized Gulf Stream or Kuroshio current. The mean of the fields, denoted with an overbar, is defined in this computation as a coarse-grained running average of 2° width.

[e.g., *Yentsch and Phinney*, 1989; *Chisholm*, 1992; *Ciotti et al.*, 2002; *Li*, 2002; *Irigoien et al.*, 2004; *Uitz et al.*, 2006]. Biomass is typically added in successively larger size classes as the total biomass increases, while smaller size classes remain relatively unchanged [*Landry*, 2002].

[31] These large-scale patterns are also seen in ecosystem responses to the episodic addition of limiting nutrients. *Cavender-Bares et al.* [2001] measured size-abundance spectra of phytoplankton in mesocosms of Sargasso Sea water enriched with NO_3 and PO_4 and found that waves of enhanced biomass propagated from small to large sizes over 5 days. Similar analyses inside iron-fertilized patches during IronEx II showed peaks and troughs of particle abundance propagating toward the larger sizes of the size spectrum over 8 days with large pennate diatoms dominating the increase in phytoplankton biomass [e.g., *Coale et al.*, 1996; *Landry et al.*, 2000]. This ecosystem response to enrichment is an emergent property driven by the size-dependencies of fundamental biological rates such as growth, production and grazing [e.g., *Rassoulzadegan and Sheldon*, 1986; *Fuchs and Franks*, 2010; *Poulin and Franks*, 2010]. Pulses of biomass propagating to larger size classes after a nutrient injection reflect changing balances of growth and predation with size and time. These imbalances can lead to disproportionate growth of larger phytoplankton and efficient food chains fueling pelagic fish production [e.g., *Moloney and Field*, 1991]. They can also lead to episodic particle fluxes and locally enhanced carbon sequestration [e.g., *Guidi et al.*, 2007]. It is thus critical to measure and understand the size-dependencies of phytoplankton growth and microzooplankton grazing rates in submesoscale features where such pulses may be focused.

[32] The changes in the size structure of the planktonic community driven by nutrient pulses will lead to local patches of distinct species abundances. Such patches will become stirred and distorted by the mesoscale and submesoscale horizontal velocity fields [*Martin et al.*, 2001]. By combining multisatellite data, notably high-resolution ocean-colour maps of dominant phytoplankton types and altimetry-derived Lagrangian diagnostics of the surface transport, *d'Ovidio et al.* [2010] demonstrated that the phytoplankton landscape is organized into submesoscale patches, often dominated by a particular phytoplankton group, separated by physical fronts induced by horizontal stirring. These physical fronts effectively delimit ephemeral ecological niches by encircling water masses of similar history and whose lifetimes are comparable to the timescale of the biological response (a few weeks). This submesoscale structuring of the plankton community is a direct consequence of horizontal stirring by the turbulent circulation.

4.1. Size-Dependent Ecosystem Response to a Nutrient Pulse

[33] To explore the size-dependent community response to a nutrient pulse, we used the *Poulin and Franks* [2010, hereinafter PF10] size-structured ecosystem model, which allows for an arbitrary number of different size classes of phytoplankton P and zooplankton Z (typically >500 size classes of each). The model is similar to the *Fuchs and*

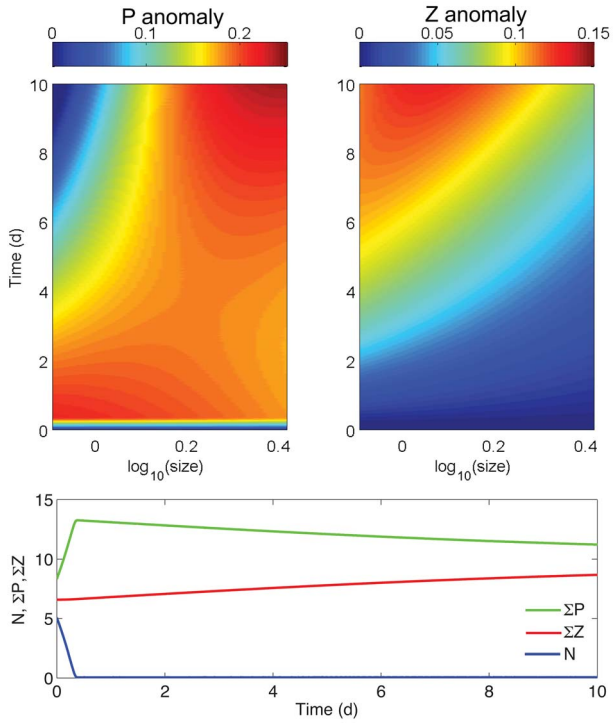

Figure 5. Response of size-structured ecosystem to a nutrient pulse at time 0. (top left) Phytoplankton biomass anomalies (log10 of the ratio of the time-dependent distribution to the initial distribution). (top right) Zooplankton biomass anomalies. (bottom) Time series of nutrients, total phytoplankton, and total zooplankton. Model is a time-dependent version of PF10. In the first 4 days after the nutrient pulse the smallest phytoplankton bloom, followed by an increase of their grazers. The grazer control of the smallest phytoplankton allows the larger phytoplankton to bloom. This bloom slowly propagates to the largest phytoplankton. Each bloom is followed by an increase in population of that size class's grazers. Note the rapid uptake of the nutrient pulse.

Franks [2010] size-structured model: it is based on a simple NPZ model structure, but includes potential size-dependence of all biological processes (growth, grazing, assimilation efficiency, etc.). The results shown here were obtained with a herbivore-only model.

[34] The PF10 model was initialized at steady state with a total nutrient concentration (phytoplankton+zooplankton +dissolved nutrients) of 10 mmolN m^{-3} and given a nutrient pulse of 5 mmolN m^{-3} over 1 day (Figure 5). There was an immediate growth response across all phytoplankton size classes. Over the days following the initial response, the smallest phytoplankton showed the largest increase in biomass, followed by an increase in the biomass of their grazers. The increase of the grazers led to eventual net decreases in the smallest phytoplankton. This grazer-induced decrease in the smallest phytoplankton decreased their competitive ability, allowing growth of the larger phytoplankton. Over the next 10 days (and longer), a pulse of high biomass propagated from the smallest phytoplankton toward the largest. The duration of the biomass pulse depends on the phytoplankton growth and zooplankton grazing rates; the pulse propagates more slowly and is of longer duration as it reaches the larger (slower-growing) phytoplankton. The phytoplanktonic biomass pulse in a given size class is ultimately terminated by a subsequent biomass increase of the herbivores. These results suggest that in a Lagrangian sense, nutrient pulses to the euphotic zone should lead to a patchy, distinct, and evolving planktonic community structure compared to surrounding waters. The resonance between the time scales of submesoscale-driven nutrient injections (O(1) day [e.g., *D'Asaro et al.*, 2011]) and phytoplankton and protist grazer growth rates (O(1) d^{-1}) are expected to lead to significant modification of the planktonic community and its dynamics in the vicinity of submesoscale features.

4.2. Spatial Diversity Driven by Submesoscale Nutrient Pump

[35] The PF10 model is presently too computer intensive to run at full resolution in a 3D submesoscale-resolving model. To investigate the effects of submesoscale dynamics on spatial patterns of phytoplankton diversity, a reduced NPPZD (nutrient-phytoplankton-phytoplankton-zooplankton-detritus) model was run with a SQG (surface quasi-geostrophic) physical model [*Perruche et al.*, 2011]. In this model the phytoplankton community comprises two size classes of phytoplankton (P_1 and P_2), representing nano and micro phytoplankton respectively, using the *Moloney and Field* [1991] parameterization of growth rates. In particular, because of competitive exclusion there is no region of the parameter space (total nutrient C_o vs. irradiance I) in which P_1 and P_2 can coexist at equilibrium (Figure 6c).

[36] When coupled to the SQG model, the local perturbations of nutrients by physical processes nevertheless allow the coexistence of the two phytoplankton types (Figures 6a and 6b): P_2 dominates in the long thin filaments between eddies formed by the straining of the concentration fields; P_1 dominates inside eddies, but is also found in the filaments. Both the coexistence and shifts in the balance of this coexistence over short length scales can be explained by considering the response time scales of the system (Figure 6c). The similarity between the short time scales associated with strong submesoscale vertical nutrient injections and the ecosystem response time scale (given along the red line, Figure 6c) favours dominance by the largest phytoplankton size class. On the other hand, the longer time scales associated with eddies with low rates of vertical nutrient injection favor the smallest phytoplankton class. The potential resonances between different components of the plankton and different scales of physical forcing lead to strong spatial and temporal heterogeneities in community structure and dynamics.

[37] These nascent modelling studies underscore the importance of resolving submesoscale features in models and in sampling. Biological processes such as growth, grazing, aggregation and predation are all expected to be enhanced in submesoscale upwellings. Nutrient pulses are able to propagate through the trophic web, driving strong changes in community structure. The spatial and temporal heterogeneity of nutrient pulses, combined with horizontal stirring, alters the competitive balance among different phytoplankton species. We thus expect to see strong spatial and temporal gradients in planktonic community structure forced by submesoscale physical dynamics. Furthermore, *Cotté et al.* [2011] and *Tew Kai et al.* [2009] have recently shown that the effects of submesoscale dynamics extend through the food web to affect the top predators' foraging

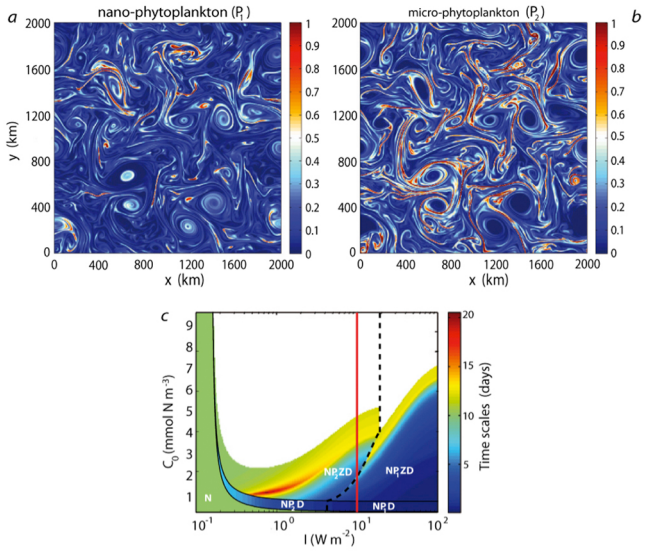

Figure 6. Spatial distribution snapshot of phytoplankton size classes (a) P_1 and (b) P_2 in a submesoscale-resolving model (colour bar in mmol N m^{-3}). (c) Equilibrium community structure under different total nitrogen (C_0) and irradiance (I) conditions (note that irradiance axis is logarithmic). White letters indicate the state variables that exist at equilibrium for the given irradiance and nutrient concentration. Note that P_1 and P_2 do not coexist at equilibrium. Time scale to reach equilibrium (in days) is indicated in colours (white area corresponds to limit cycles at equilibrium). Dashed line separates the two regions in which either P_1 or P_2 exists at equilibrium. Red line indicates the position in the parameter space corresponding to the SQG simulation with a fixed irradiance level of 10 Wm^{-2} (adapted from *Perruche et al.* [2010, 2011]). The coexistence of P_1 and P_2 in the SQG model is due to the perturbations of the ecosystem by mesoscale and submesoscale motions, maintaining the ecosystem out of equilibrium.

behaviour. Thus, the combined effects of submesoscale features, even though a relatively small fraction of the total area, may be disproportionately important to biological dynamics.

5. Observational Considerations

[38] A major obstacle to testing current predictions from theories and models is the difficulty of adequately sampling the submesoscale. As mentioned above, the phenomena of interest are both ephemeral and localized, taking just a few days to wax and wane and only being of O(1–10) km in width despite being up to hundreds of kilometers in length. A major aspect of the observational challenge, therefore, is one common to the purely physical study of the submesoscale: the need to be able to survey a region at sufficiently high temporal and spatial resolution.

[39] Gliders (e.g., SPRAY spray.ucsd.edu/pub/rel/index.php, Slocum www.webbresearch.com/slocumglider.aspx, Seaglider www.irobot.com/gi/maritime/1KA_Seaglider) are fast becoming the platform of choice in a wide range of oceanographic applications. Typically a glider can cover 1 km horizontally in an hour with an ascent angle of around one in five. Steeper angles of ascent are possible but with the consequence of slower horizontal progress. Even for larger submesoscale features of O(10) km width a glider would require half a day for one transect. The slow speed also means that the strong directional currents associated with many of the submesoscale features of interest have the potential to displace the glider significantly over even one transect.

[40] A more traditional alternative is a ship-towed undulating device, such as the SeaSoar [*Pidcock*, 2011] or Triaxus [*D'Asaro et al.*, 2011] platforms. These allow sampling typically 10–20 times faster than a glider, permitting much better time resolution of the evolution of submesoscale features. Furthermore, the physical connection to the ship allows the use of sensors whose power demands would significantly curtail the range of a glider. The costs of and demands on research vessels mean that such studies are nevertheless limited in duration relative to gliders, which can continue to sample a region for months even during the winter period.

[41] The relevant submesoscale timescales for a study impose other constraints on a study of their biogeochemistry. An obvious intention might be to record biogeochemical processes such as primary production and export of carbon over an annual cycle at a resolution sufficient to allow the contribution of the submesoscale to be assessed. Given the fleeting existence of any specific submesoscale feature this annual budget may best be addressed using Eulerian sampling, building up a statistical picture of the cumulative effect of submesoscale processes at a fixed location. The problem then arises of how temporal signals in biogeochemistry can be disentangled from simple advection of spatial variability through the site. Having a collection of moorings spaced at distances sufficient to resolve submesoscale spatial variability might be one approach. The spatial coverage would also be required to separate out the regional change in time associated with biological processes such as nutrient uptake, population growth and sedimentation. This approach to studying the underlying physical processes of the submesoscale is to be tried, for example, by the UK OSMOSIS program, with the moorings augmented by gliders.

[42] If study of the dynamics associated with a specific submesoscale feature is of interest then a Lagrangian approach is required, as the mesoscale circulation may advect any feature tens of kilometers in just one day. For example, *D'Asaro et al.* [2011] used a neutrally buoyant float to mark a submesoscale front in the Japan Sea. They used this as a moving reference point for repeated Triaxus surveys of the physical characteristics. A similar observational strategy, augmented with fluorescence and backscattering measurements, was followed during the 2008 North Atlantic spring bloom experiment [*Fennel et al.*, 2011; *Alkire et al.*, 2012; E. D'Asaro, personal communication, 2011]. A major program of the US Office of Naval Research targeting the physics of the submesoscale will also use a Lagrangian approach. Two recent developments that show considerable potential for Lagrangian studies involve the use of multiple drifters. The Autonomous Underwater Explorer (http://jaffeweb.ucsd.edu/node/81) is a very compact (2 L) float with active buoyancy control that can carry multiple biogeochemical sensors and can be deployed in groups, collecting information on spatial variability through triangulation by means of acoustic communication links as they

disperse. A similar idea lies behind the Wire Walker [*Rainville and Pinkel*, 2001; *Pinkel et al.*, 2011] which maintains a float at the surface but uses wave power to constantly yo-yo a sensor package beneath it. Deploying a number of these would provide a high-frequency and irregularly spaced but 3D map of biogeochemical and physical processes. These vehicles can collect complete vertical profiles through 250 m of water with less than 10 minutes between profiles; the time scales are shorter if the profiling depth is decreased.

[43] Current satellite altimeters do not resolve the submesoscale, but do provide information on the mesoscale field which can be used to diagnose where submesoscale fronts [*d'Ovidio et al.*, 2004, 2009; *Lehahn et al.*, 2007; *Desprès et al.*, 2011] and submesoscale vertical transport [*Legal and Tréguier*, 2007; *Isern-Fontanet et al.*, 2008] should occur. The Indo-German LOHAFEX iron fertilization experiment (March 2009) and French KEOPS2 natural fertilization experiment in the Southern Ocean (Nov 2011) used an innovative sampling strategy based on this concept, with real-time identification of transport structures from the analysis of multi-satellite altimetry data and surface buoy release. This approach is aimed at identifying environments naturally isolated by the structure of the surface circulation, where it becomes possible to study the time evolution of biophysical processes in a Lagrangian sense. More generally, the use of altimetry should soon become common practice to adjust sampling strategy at sea in real time (for instance, with repeated sections across submesoscale fronts, as in *Legal et al.* [2007]) according to the position of the frontal structures that can be forecast with such data. In the near future, development of wide-swath altimetry by both the NASA SWOT and ESA Wavemill programs would take the spatial resolution of geostrophic currents to a few km, which should significantly improve our ability to identify in real time where submesoscale fronts may be generated.

[44] Colour satellites have long provided information on phytoplankton distributions at a resolution capable of resolving the submesoscale [e.g., *Gower et al.*, 1980], though such information is often discarded by averaging the data into weekly or monthly composites. Recent developments using satellites to study the biogeochemistry of the submesoscale in more detail include nitrate estimates [*Goes et al.*, 2004] and algorithms to probe community composition by using the array of frequencies on multi-spectral sensors to fuller extent [e.g., *Alvain et al.*, 2005; *Uitz et al.*, 2010]. One concern with the former is that the nitrate algorithm is based on sea-surface temperature and chlorophyll measurements, so it could be argued that it is not an independent measurement. It would additionally need to be ascertained whether the empirical relationship underpinning it holds at the submesoscale where biogeochemistry will often be far out of equilibrium. There is also the question of whether, to obtain an acceptable signal to noise ratio, it would be necessary to spatially average the signal up to scales that would preclude the submesoscale from being resolved accurately. Nevertheless, if it proves possible to allay such concerns, the approach is an appealing one as it potentially allows a much more thorough mapping of the surface nitrate field than could be achieved by any ship or glider survey at a resolution which should capture much of the submesoscale variability.

[45] Returning to *in situ* observations, it has long been a problem that very few biogeochemical properties can be accurately measured using compact autonomous sensors. It is only recently that ultraviolet-based sensors capable of robust measurements of nitrate with a sensitivity suitable for open ocean biogeochemistry have been developed [*Pidcock et al.*, 2010; *Johnson et al.*, 2010]. The most exciting development for submesoscale studies, perhaps, is the emergence of lab-on-chip technology; the ability to use advanced engineering techniques to build low energy, sophisticated but small sensors, with obvious potential for deployment on any of the platforms discussed above. Of particular relevance to submesoscale biogeochemistry are wave-guide-based sensors for a range of nutrients [*Adornato et al.*, 2009]; miniaturized flow cytometers [e.g., *Barat et al.*, 2010] and species-specific RNA probes [e.g., *Tsaloglou et al.*, 2011]. The latter two in particular offer huge potential for starting to tease apart the complexities of community composition at the submesoscale.

6. Conclusions

[46] Submesoscale dynamics dominate at time and space scales that make them uniquely important to the structure and functioning of planktonic ecosystems. Resulting from interactions within the mesoscale eddy field, submesoscale flows can generate intense vertical motions at fronts, driving nutrients into the euphotic zone, and subducting organic carbon beneath it. The efficacy of submesoscale dynamics in influencing primary production and ecosystem structure depends on the local hydrography, euphotic depth, and nutrient distributions. Our lack of knowledge of the physical flows and biogeochemical responses at the submesoscale is due both to their dynamic complexity, and the practical difficulties in sampling at the appropriate time and space scales. However, recent advances in physical models, planktonic ecosystem models and ocean sampling technologies makes this an ideal time to explore the physical-chemical-biological interactions at these scales. In particular we need to gain understanding of how the intense vertical motions at the submesoscale contribute to regional-average properties such as vertical carbon and nitrogen fluxes. The strong spatial patchiness in planktonic community structure induced by submesoscale motions may lead to a significant fraction of the vertical flux being restricted to similarly small spatial and temporal scales—scales that would be missed by measurements that average over inappropriately large spatial and temporal scales. Improved understanding of the importance of submesoscale dynamics will come only through targeted interdisciplinary field and modelling programs.

[47] **Acknowledgments.** All authors contributed equally to this paper. This review builds on the outcomes of a conference funded by EUR-OCEANS and Europôle Mer: *Influence of meso- and sub-mesoscale ocean dynamics on the global carbon cycle and marine ecosystems*, Centre de la Mer, Aber Wrac'h, France, June 2010. This work was supported by the joint CNRS-INSU-LEFE program & EUR-OCEANS flagship "TANGGO" (Lévy, Rivière, Martin), by the CCE-LTER program (Franks, Rivière), by NSF award 1155205 (Ferrari) and by the NERC Oceans 2025 program (Martin).

[48] The Editor thanks Amala Mahadevan and an anonymous reviewer for assisting in the evaluation of this paper.

References

Adornato, L., A. Cardenas-Valencia, E. Kaltenbacher, R. H. Byrne, K. Daly, K. Larkin, S. Hartman, M. Mowlem, R. D. Prien, and V. C.

Garçon (2009), In situ nutrient sensors for ocean observing systems, in *Proceedings of the Oceanobs'09: Sustained Ocean observations and Information for Society Conference (Vol. 2), Venice, Italy, 21–25 September 2009*, edited by J. Hall, D. E. Harrison, and D. Stammer, *ESA Publ.*, *WPP-306*, doi:10.5270/OceanObs09.cwp.01.

Alkire, M. B., et al. (2012), Estimates of net community production and export using high-resolution, Lagrangian measurements of O_2, NO_3^-, and POC through the evolution of a spring diatom bloom in the North Atlantic, *Deep Sea Res., Part I*, *64*, 157–174, doi:10.1016/j.dsr.2012.01.012.

Allen, J., L. Brown, R. Sanders, C. Moore, A. Mustard, S. Fielding, M. Lucas, M. Rixen, G. Savidge, and S. Henson (2005), Diatom carbon export enhanced by silicate upwelling in the northeast Atlantic, *Nature*, *437*, 728–732, doi:10.1038/nature03948.

Alvain, S., C. Moulin, Y. Dandonneau, and F. M. Bréon (2005), Remote sensing of phytoplankton groups in case 1 waters from global SeaWiFS imagery, *Deep Sea Res., Part I*, *52*, 1989–2004, doi:10.1016/j.dsr.2005.06.015.

Barat, D., G. Benazzi, M. Mowlem, J. M. Ruano, and H. Morgan (2010), Design, simulation and characterisation of integrated optics for a microfabricated flow cytometer, *Opt. Commun.*, *283*(9), 1987–1992, doi:10.1016/j.optcom.2009.12.046.

Boccaletti, G., R. Ferrari, and B. Fox-Kemper (2007), Mixed layer instabilities and restratification, *J. Phys. Oceanogr.*, *37*, 2228–2250, doi:10.1175/JPO3101.1.

Calil, P. H. R., and K. J. Richards (2010), Transient upwelling hot spots in the oligotrophic North Pacific, *J. Geophys. Res.*, *115*, C02003, doi:10.1029/2009JC005360.

Capet, X., J. McWilliams, M. Molemaker, and A. Shchepetkin (2008), Mesoscale to submesoscale transition in the California Current system. Part I: Flow structure, eddy flux, and observational tests, *J. Phys. Oceanogr.*, *38*, 29–43, doi:10.1175/2007JPO3671.1.

Cavender-Bares, K. K., A. Rinaldo, and S. W. Chisholm (2001), Microbial size spectra from natural and nutrient enriched ecosystems, *Limnol. Oceanogr.*, *46*, 778–789, doi:10.4319/lo.2001.46.4.0778.

Charney, J. G. (1971), Geostrophic turbulence, *J. Atmos. Sci.*, *28*, 1087–1095, doi:10.1175/1520-0469(1971)028<1087:GT>2.0.CO;2.

Chelton, D. B., R. A. Deszoeke, and M. G. Schlax (1998), Geographical variability of the first baroclinic Rossby radius of deformation, *J. Phys. Oceanogr.*, *28*, 433–460, doi:10.1175/1520-0485(1998)028<0433:GVOTFB>2.0.CO;2.

Chelton, D. B., P. Gaube, M. G. Schlax, J. J. Early, and R. M. Samelson (2011), The influence of nonlinear mesoscale eddies on near-surface oceanic chlorophyll, *Science*, *334*, 328–332, doi:10.1126/science.1208897.

Chisholm, S. W. (1992), Phytoplankton size, in *Primary Productivity and Biogeochemical Cycles in the Sea*, edited by P. G. Falkowski and A. D. Woodhead, pp. 213–237, Plenum, New York.

Ciotti, A. M., M. R. Lewis, and J. J. Cullen (2002), Assessment of the relationships between dominant cell size in natural phytoplankton communities and the spectral shape of the absorption coefficient, *Limnol. Oceanogr.*, *47*, 404–417, doi:10.4319/lo.2002.47.2.0404.

Cipollini, P., et al. (2001), Rossby waves detected in global ocean colour data, *Geophys. Res. Lett.*, *28*, 323–326, doi:10.1029/1999GL011231.

Coale, K. H., et al. (1996), A massive phytoplankton bloom induced by an ecosystem-scale iron fertilization experiment in the equatorial Pacific Ocean, *Nature*, *383*, 495–501, doi:10.1038/383495a0.

Cotté, C., F. d'Ovidio, A. Chaigneau, M. Lévy, I. Taupier-Letage, B. Maté, and C. Guinet (2011), Scale-dependent interactions of Mediterranean whales with marine dynamics, *Limnol. Oceanogr.*, *56*(1), 219–232, doi:10.4319/lo.2011.56.1.0219.

D'Asaro, E., C. Lee, L. Rainville, R. Harcourt, and L. Thomas (2011), Enhanced turbulence and energy dissipation at ocean fronts, *Science*, *332*(6027), 318–322, doi:10.1126/science.1201515.

d'Ovidio, F., C. López, E. Hernández-García, and V. Fernández (2004), Mixing structures in the Mediterranean Sea from finite-size Lyapunov exponents, *Geophys. Res. Lett.*, *31*, L17203, doi:10.1029/2004GL020328.

d'Ovidio, F., J. Isern-Fontanet, C. Lopez, E. Hernandez-García, and E. Garcia-Ladona (2009), Comparison between Eulerian diagnostics and finite-size Lyapunov exponents computed from altimetry in the Algerian basin, *Deep Sea Res., Part I*, *56*, 15–31, doi:10.1016/j.dsr.2008.07.014.

d'Ovidio, F., S. De Monte, S. Alvain, Y. Dandonneau, and M. Lévy (2010), Fluid dynamical niches of phytoplankton types, *Proc. Natl. Acad. Sci. U. S. A.*, *107*, 18,366–18,370, doi:10.1073/pnas.1004620107.

Desprès, A., G. Reverdin, and F. D'Ovidio (2011), Mechanisms and spatial variability of meso scale frontogenesis in the northwestern subpolar gyre, *Ocean Modell.*, *39*, 97–113, doi:10.1016/j.ocemod.2010.12.005.

Falkowski, P., D. Ziemann, Z. Kolber, and P. K. Bienfang (1991), Role of eddy pumping in enhancing primary production in the ocean, *Nature*, *352*, 55–58, doi:10.1038/352055a0.

Fennel, K., I. Cetinić, E. D'Asaro, C. Lee, and M. J. Perry (2011), Autonomous data describe North Atlantic spring bloom, *Eos Trans. AGU*, *92*(50), 465, doi:10.1029/2011EO500002.

Ferrari, R. (2011), A frontal challenge for climate models, *Science*, *332*, 316–317, doi:10.1126/science.1203632.

Ferrari, R., J. C. McWilliams, V. Canuto, and D. Dubovikov (2008), Parameterization of eddy fluxes at the ocean boundaries, *J. Clim.*, *21*, 2770–2789, doi:10.1175/2007JCLI1510.1.

Fielding, S., et al. (2001), Mesoscale subduction at the Almeria-Oran front. Part 2: Biophysical interactions, *J. Mar. Syst.*, *30*(3–4), 287–304, doi:10.1016/S0924-7963(01)00063-X.

Flierl, G. R., and C. S. Davis (1993), Biological effects of Gulf stream meandering, *J. Mar. Res.*, *51*, 529–560, doi:10.1357/0022240933224016.

Fox-Kemper, B., R. Ferrari, and R. Hallberg (2008), Parameterization of mixed layer eddies. I: Theory and diagnosis, *J. Phys. Oceanogr.*, *38*, 1145–1165, doi:10.1175/2007JPO3792.1.

Franks, P. J. S., and L. J. Walstad (1997), Phytoplankton patches at fronts: A model of formation and response to transient wind events, *J. Mar. Res.*, *55*, 1–29, doi:10.1357/0022240973224472.

Fuchs, H. L., and P. J. S. Franks (2010), Plankton community properties determined by nutrients and size-selective feeding, *Mar. Ecol. Prog. Ser.*, *413*, 1–15, doi:10.3354/meps08716.

Goes, J. I., H. do R. Gomes, T. Saino, C. S. Wong, and C. W. Mordy (2004), Exploiting MODIS data for estimating sea surface nitrate from space, *Eos Trans. AGU*, *85*(44), 449, doi:10.1029/2004EO440001.

Gower, J., K. Denman, and R. Holyer (1980), Phytoplankton patchiness indicates the fluctuation spectrum of mesoscale oceanic structure, *Nature*, *288*, 157–159, doi:10.1038/288157a0.

Gruber, N., et al. (2011), Eddy-induced reduction of biological production in eastern boundary upwelling systems, *Nat. Geosci.*, *4*, 787–792, doi:10.1038/ngeo1273.

Guidi, L., L. Stemmann, L. Legendre, M. Picheral, L. Prieur, and G. Gorsky (2007), Vertical distribution of aggregates (>100 mm) and mesoscale activity in the northeastern Atlantic: Effects on the deep vertical export of surface carbon, *Limnol. Oceanogr.*, *52*, 7–18, doi:10.4319/lo.2007.52.1.0007.

Holloway, G., and K. L. Denman (1989), Influence of internal waves on primary production, *J. Plankton Res.*, *11*, 409–413, doi:10.1093/plankt/11.2.409.

Hoskins, B. J. (1982), The mathematical theory of frontogenesis, *Annu. Rev. Fluid Mech.*, *14*, 131–151, doi:10.1146/annurev.fl.14.010182.001023.

Hoskins, B. J., and F. P. Bretherton (1972), Atmospheric frontogenesis models: Mathematical formulation and solution, *J. Atmos. Sci.*, *29*, 11–37, doi:10.1175/1520-0469(1972)029<0011:AFMMFA>2.0.CO;2.

Irigoien, X., J. Huisman, and R. P. Harris (2004), Global biodiversity patterns of marine phytoplankton and zooplankton, *Nature*, *429*, 863–867, doi:10.1038/nature02593.

Isern-Fontanet, J., G. Lapeyre, P. Klein, B. Chapron, and M. W. Hect (2008), Three-dimensional reconstruction of oceanic mesoscale currents from surface information, *J. Geophys. Res.*, *113*, C09005, doi:10.1029/2007JC004692.

Johnson, K. S., S. C. Riser, and D. M. Karl (2010), Nitrate supply from deep to near-surface waters of the North Pacific subtropical gyre, *Nature*, *465*, 1062–1065, doi:10.1038/nature09170.

Joyce, T. M., L. N. Thomas, and F. Bahr (2009), Wintertime observations of Subtropical Mode Water formation within the Gulf Stream, *Geophys. Res. Lett.*, *36*, L02607, doi:10.1029/2008GL035918.

Kadko, D., L. Washburn, and B. H. Jones (1991), Evidence of subduction within cold filaments of the N. California Coastal Transition Zone, *J. Geophys. Res.*, *96*, 14,909–14,926, doi:10.1029/91JC00885.

Karleskind, P., M. Lévy, and L. Mémery (2011a), Modifications of mode water properties by sub-mesoscales in a bio-physical model of the northeast Atlantic, *Ocean Modell.*, *39*, 47–60, doi:10.1016/j.ocemod.2010.12.003.

Karleskind, P., M. Lévy, and L. Memery (2011b), Subduction of carbon, nitrogen, and oxygen in the northeast Atlantic, *J. Geophys. Res.*, *116*, C02025, doi:10.1029/2010JC006446.

Klein, P., and G. Lapeyre (2009), The oceanic vertical pump induced by mesoscale and submesoscale turbulence, *Annu. Rev. Mar. Sci.*, *1*, 351–375, doi:10.1146/annurev.marine.010908.163704.

Klein, P., B. Hua, G. Lapeyre, X. Capet, S. L. Gentil, and H. S. Sasaki (2008), Upper ocean turbulence from high 3-D resolution simulations, *J. Phys. Oceanogr.*, *38*, 1748–1763, doi:10.1175/2007JPO3773.1.

Landry, M. R. (2002), Integrating classical and microbial food web concepts: Evolving views from the open-ocean tropical Pacific, *Hydrobiologia*, *480*, 29–39, doi:10.1023/A:1021272731737.

Landry, M. R., M. E. Ondrusek, S. J. Tanner, S. L. Brown, J. Constantinou, R. R. Bidigare, K. H. Coale, and S. Fitzwater (2000), Biological response to iron fertilization in the eastern equatorial Pacific (IronEx II).

I. Microplankton community abundances and biomass, *Mar. Ecol. Prog. Ser.*, *201*, 27–42, doi:10.3354/meps201027.

Lapeyre, G., and P. Klein (2006), Impact of the small scale elongated filaments on the oceanic vertical pump, *J. Mar. Res.*, *64*, 835–851, doi:10.1357/002224006779698369.

Lapeyre, G., P. Klein, and L. Hua (2006), Oceanic restratification by surface frontogenesis, *J. Phys. Oceanogr.*, *36*, 1577–1590, doi:10.1175/JPO2923.1.

Lathuilière, C., V. Echevin, M. Lévy, and G. Madec (2010), On the role of mesoscale circulation on an idealized coastal upwelling ecosystem, *J. Geophys. Res.*, *115*, C09018, doi:10.1029/2009JC005827.

Lathuilière, C., M. Lévy, and V. Echevin (2011), Impact of eddy-driven vertical fluxes on phytoplankton abundance in the euphotic layer, *J. Plankton Res.*, *33*(5), 827–831, doi:10.1093/plankt/fbq131.

Ledwell, J. R., A. J. Watson, and C. S. Law (1998), Mixing of a tracer in the pycnocline, *J. Geophys. Res.*, *103*(C10), 21,499–21,529, doi:10.1029/98JC01738.

Legal, C., P. Klein, A.-M. Trèguier, and J. Paillet (2007), Diagnosis of the vertical motions in a mesoscale stirring region, *J. Phys. Oceanogr.*, *37*, 1413–1424, doi:10.1175/JPO3053.1.

Lehahn, Y., F. d'Ovidio, M. Lévy, and E. Heitzel (2007), Stirring of the northeast Atlantic spring bloom: A Lagrangian analysis based on multi-satellite data, *J. Geophys. Res.*, *112*, C08005, doi:10.1029/2006JC003927.

Lehahn, Y., F. d'Ovidio, M. Lévy, Y. Amitai, and E. Heifetz (2011), Long range transport of a quasi isolated chlorophyll patch by an Aghulas ring, *Geophys. Res. Lett.*, *38*, L16610, doi:10.1029/2011GL048588.

Lévy, M. (2003), Mesoscale variability of phytoplankton and of new production: Impact of the large-scale nutrient distribution, *J. Geophys. Res.*, *108*(C11), 3358, doi:10.1029/2002JC001577.

Lévy, M., L. Mémery, and G. Madec (1998), The onset of a bloom after deep winter convection in the north western Mediterranean Sea: Mesoscale process study with a primitive equation model, *J. Mar. Syst.*, *16*, 7–21, doi:10.1016/S0924-7963(97)00097-3.

Lévy, M., M. Visbeck, and N. Naik (1999), Sensitivity of primary production to different eddy parameterizations: A case study of the spring bloom development in the north western Mediterranean Sea, *J. Mar. Res.*, *57*, 427–448, doi:10.1357/002224099764805147.

Lévy, M., L. Mémery, and G. Madec (2000), Combined effects of mesoscale processes and atmospheric high-frequency variability on the spring bloom in the MEDOC area, *Deep Sea Res., Part I*, *47*, 27–53, doi:10.1016/S0967-0637(99)00051-5.

Lévy, M., P. Klein, and A.-M. Tréguier (2001), Impact of submesoscale physics on production and subduction of phytoplankton in an oligotrophic regime, *J. Mar. Res.*, *59*, 535–565, doi:10.1357/002224001762842181.

Lévy, M., M. Gavart, L. Mémery, G. Caniaux, and A. Paci (2005), A four-dimensional mesoscale map of the spring bloom in the northeast Atlantic (POMME experiment): Results of a prognostic model, *J. Geophys. Res.*, *110*, C07S21, doi:10.1029/2004JC002588.

Lévy, M., P. Klein, and M. B. Jelloul (2009), New production stimulated by high-frequency winds in a turbulent mesoscale eddy field, *Geophys. Res. Lett.*, *36*, L16603, doi:10.1029/2009GL039490.

Lévy, M., P. Klein, A.-M. Tréguier, D. Iovino, G. Madec, S. Masson, and K. Takahashi (2010), Modifications of gyre circulation by sub-mesoscale physics, *Ocean Modell.*, *34*, 1–15, doi:10.1016/j.ocemod.2010.04.001.

Lévy, M., D. Iovino, L. Resplandy, P. Klein, A.-M. Tréguier, G. Madec, S. Masson, and K. Takahashi (2012), Large-scale impacts of submesoscale dynamics on phytoplankton: Local and remote effects, *Ocean Modell.*, *43-44*, 77–93, doi:10.1016/j.ocemod.2011.12.003.

Lewis, M. R., et al. (1986), Vertical nitrate fluxes in the oligotrophic ocean, *Science*, *234*, 870–873, doi:10.1126/science.234.4778.870.

Li, W. K. W. (2002), Macroecological patterns of phytoplankton in the northwestern North Atlantic Ocean, *Nature*, *419*, 154–157, doi:10.1038/nature00994.

Mahadevan, A., and D. Archer (2000), Modelling the impact of fronts and mesoscale circulation on the nutrient supply and biogeochemistry of the upper ocean, *J. Geophys. Res.*, *105*, 1209–1225, doi:10.1029/1999JC900216.

Mahadevan, A., and A. Tandon (2006), An analysis of mechanisms for submesoscale vertical motion at ocean fronts, *Ocean Modell.*, *14*(3–4), 241–256, doi:10.1016/j.ocemod.2006.05.006.

Mahadevan, A., M. Lévy, and L. Mémery (2004), Mesoscale variability of sea surface pCO_2: What does it respond to?, *Global Biogeochem. Cycles*, *18*, GB1017, doi:10.1029/2003GB002102.

Mahadevan, A., A. Tagliabue, L. Bopp, A. Lenton, L. Mémery, and M. Lévy (2011), Impact of episodic vertical fluxes on sea surface pCO_2, *Philos. Trans. R. Soc. A*, *369*, 2009–2025, doi:10.1098/rsta.2010.0340.

Martin, A. P. (2003), Phytoplankton patchiness: The role of lateral stirring and mixing, *Prog. Oceanogr.*, *57*(2), 125–174, doi:10.1016/S0079-6611(03)00085-5.

Martin, A. P., and P. Pondaven (2003), On estimates for the vertical nitrate flux due to eddy pumping, *J. Geophys. Res.*, *108*(C11), 3359, doi:10.1029/2003JC001841.

Martin, A. P., and K. J. Richards (2001), Mechanisms for vertical nutrient transport within a North Atlantic mesoscale eddy, *Deep Sea Res., Part II*, *48*(4–5), 757–773, doi:10.1016/S0967-0645(00)00096-5.

Martin, A. P., K. J. Richards, and M. J. R. Fasham (2001), Phytoplankton production and community structure in an unstable frontal region, *J. Mar. Syst.*, *28*(1–2), 65–89, doi:10.1016/S0924-7963(00)00084-1.

Martin, A. P., K. J. Richards, A. Bracco, and A. Provenzale (2002), Patchy productivity in the open ocean, *Global Biogeochem. Cycles*, *16*(2), 1025, doi:10.1029/2001GB001449.

McGillicuddy, D. J., A. R. Robinson, D. A. Siegel, H. W. Jannasch, R. Johnson, T. D. Dickey, J. McNeil, A. F. Michaels, and A. H. Knap (1998), Influence of mesoscale eddies on new production in the Sargasso Sea, *Nature*, *394*, 263–266, doi:10.1038/28367.

McGillicuddy, D. J., L. A. Anderson, S. C. Doney, and M. E. Maltrud (2003), Eddy-driven sources and sinks of nutrients in the upper ocean: Results from a 0.1 degree resolution model of the North Atlantic, *Global Biogeochem. Cycles*, *17*(2), 1035, doi:10.1029/2002GB001987.

McGillicuddy, D. J., et al. (2007), Eddy/wind interactions stimulate extraordinary mid-ocean plankton blooms, *Science*, *316*, 1021–1026, doi:10.1126/science.1136256.

McWilliams, J. C. (2010), A perspective on submesoscale geophysical turbulence, in *IUTAM Symposium on Turbulence in the Atmosphere and Oceans*, edited by D. Dritschedl, pp. 131–141, Springer, Dordrecht, Netherlands.

Molemaker, M. J., J. C. McWilliams, and X. Capet (2010), Balanced and unbalanced routes to dissipation in an equilibrated Eady flow, *J. Fluid Mech.*, *654*, 35–63, doi:10.1017/S0022112009993272.

Moloney, C. L., and J. G. Field (1991), The size-based dynamics of plankton food webs. I. A simulation model of carbon and nitrogen flows, *J. Plankton Res.*, *13*, 1003–1038, doi:10.1093/plankt/13.5.1003.

Nagai, T., A. Tandon, N. Gruber, and J. McWilliams (2008), Biological and physical impacts of ageostrophic frontal circulations driven by confluent flow and vertical mixing, *Dyn. Atmos. Oceans*, *45*, 229–251, doi:10.1016/j.dynatmoce.2007.12.001.

Niewiadomska, K., H. Claustre, L. Prieur, and F. D'Ortenzio (2008), Submesoscale physical-biogeochemical coupling across the Ligurian Current (northwestern Mediterranean) using a bio-optical glider, *Limnol. Oceanogr.*, *53*, 2210–2225, doi:10.4319/lo.2008.53.5_part_2.2210.

Oschlies, A. (2002), Can eddies make ocean deserts bloom?, *Global Biogeochem. Cycles*, *16*(4), 1106, doi:10.1029/2001GB001830.

Oschlies, A., and V. Garcon (1998), Eddy-induced enhancement of primary production in a model of the North Atlantic Ocean, *Nature*, *394*, 266–269, doi:10.1038/28373.

Pasquero, C., A. Bracco, and A. Provenzale (2005), Impact of the spatiotemporal variability of the nutrient flux on primary productivity in the ocean, *J. Geophys. Res.*, *110*, C07005, doi:10.1029/2004JC002738.

Perruche, C., P. Rivière, P. Pondaven, and X. Carton (2010), Phytoplankton competition and coexistence: Intrinsic ecosystem dynamics and impact of vertical mixing, *J. Mar. Syst.*, *81*, 99–111, doi:10.1016/j.jmarsys.2009.12.006.

Perruche, C., P. Rivière, G. Lapeyre, X. Carton, and P. Pondaven (2011), Effects of SQG turbulence on phytoplankton competition and coexistence, *J. Mar. Res.*, *69*, 105–135, doi:10.1357/002224011798147606.

Pidcock, R. (2011), Biophysical interactions in the upper ocean, PhD thesis, 242 pp., Sch. of Ocean and Earth Sci., Univ. of Southampton, Southampton, U. K.

Pidcock, R., M. Srokosz, J. Allen, M. Hartman, S. Painter, M. Mowlem, D. Hydes, and A. Martin (2010), A novel integration of an ultraviolet nitrate sensor on board a towed vehicle for mapping open-ocean submesoscale nitrate variability, *J. Atmos. Oceanic Technol.*, *27*(8), 1410–1416, doi:10.1175/2010JTECHO780.1.

Pinkel, R., M. A. Goldin, J. A. Smith, O. M. Sun, A. A. Aja, M. N. Bui, and T. Hughen (2011), The Wirewalker: A vertically profiling instrument carrier powered by ocean waves, *J. Atmos. Oceanic Technol.*, *28*, 426–435, doi:10.1175/2010JTECHO805.1.

Poulin, F. J., and P. J. S. Franks (2010), Size-structured planktonic ecosystems: Constraints, controls and assembly instructions, *J. Plankton Res.*, *32*, 1121–1130, doi:10.1093/plankt/fbp145.

Rainville, L., and R. Pinkel (2001), Wirewalker: An autonomous wave-powered vertical profiler, *J. Atmos. Oceanic Technol.*, *18*, 1048–1051, doi:10.1175/1520-0426(2001)018<1048:WAAWPV>2.0.CO;2.

Rassoulzadegan, F., and R. W. Sheldon (1986), Predator-prey interactions of nanozooplankton and bacteria in an oligotrophic marine environment, *Limnol. Oceanogr.*, *31*, 1010–1029, doi:10.4319/lo.1986.31.5.1010.

Resplandy, L., M. Lévy, F. d'Ovidio, and L. Merlivat (2009), Impact of submesoscale variability in estimating the air-sea CO_2 exchange: Results from a model study of the POMME experiment, *Global Biogeochem. Cycles*, *23*, GB1017, doi:10.1029/2008GB003239.

Rossi, V., C. Lopez, J. Sudre, E. Hernandez-Garcıa, and V. Garçon (2008), Comparative study of mixing and biological activity of the Benguela and Canary upwelling systems, *Geophys. Res. Lett.*, *35*, L11602, doi:10.1029/2008GL033610.

Ruiz, J., et al. (2004), Turbulence increases the average settling velocity of phytoplankton cells, *Proc. Natl. Acad. Sci. U. S. A.*, *101*, 17,720–17,724, doi:10.1073/pnas.0401539101.

Santoleri, R., V. Banzon, S. Marullo, E. Napolitano, F. D'Ortenzio, and R. Evans (2003), Year-to-year variability of the phytoplankton bloom in the southern Adriatic Sea (1998–2000): Sea-viewing Wide Field-of-view Sensor observations and modeling study, *J. Geophys. Res.*, *108*(C9), 8122, doi:10.1029/2002JC001636.

Spall, M. A. (1995), Frontogenesis, subduction, and cross-front exchange at upper ocean fronts, *J. Geophys. Res.*, *100*, 2543–2557, doi:10.1029/94JC02860.

Sverdrup, H. U. (1953), On the conditions for the vernal blooming of phytoplankton, *J. Cons. Int. Explor. Mer*, *18*, 287–295.

Taylor, J., and R. Ferrari (2010), Buoyancy and wind-driven convection at a mixed-layer density fronts, *J. Phys. Oceanogr.*, *40*, 1222–1242, doi:10.1175/2010JPO4365.1.

Taylor, J., and R. Ferrari (2011a), The role of density fronts in the onset of phytoplankton blooms, *Geophys. Res. Lett.*, *38*, L23601, doi:10.1029/2011GL049312.

Taylor, J., and R. Ferrari (2011b), A shutdown of turbulent convection can trigger the spring phytoplankton bloom, *Limnol. Oceanogr.*, *56*, 2293–2307, doi:10.4319/lo.2011.56.6.2293.

Tew Kai, E., V. Rossi, J. Sudre, H. Weimerskirch, C. Lopez, E. Hernandez-Garcia, F. Marsac, and V. Garçon (2009), Top marine predators track Lagrangian coherent structures, *Proc. Natl. Acad. Sci. U. S. A.*, *106*, 8245–8250, doi:10.1073/pnas.0811034106.

Thomas, L. N. (2005), Destruction of potential vorticity by winds, *J. Phys. Oceanogr.*, *35*, 2457–2466, doi:10.1175/JPO2830.1.

Thomas, L., and R. Ferrari (2008), Friction, frontogenesis, and the stratification of the surface mixed layer, *J. Phys. Oceanogr.*, *38*, 2501–2518, doi:10.1175/2008JPO3797.1.

Thomas, L. N., and T. M. Joyce (2010), Subduction on the northern and southern flanks of the gulf stream, *J. Phys. Oceanogr.*, *40*, 429–438, doi:10.1175/2009JPO4187.1.

Thomas, L. N., A. Tandon, and A. Mahadevan (2008), Submesoscale processes and dynamics, in *Eddy Resolving Ocean Modeling*, *Geophys. Monogr. Ser.*, vol. 177, edited by M. W. Hecht and H. Hasumi, pp. 17–38, AGU, Washington, D. C., doi:10.1029/177GM04.

Townsend, D. W., L. M. Cammen, P. M. Holligan, D. E. Campbell, and N. R. Pettigrew (1994), Causes and consequences of variability in the timing of spring phytoplankton blooms, *Deep Sea Res., Part I*, *41*, 747, doi:10.1016/0967-0637(94)90075-2.

Tsaloglou, M.-N., M. M. Bahi, E. M. Waugh, H. Morgan, and M. Mowlem (2011), On-chip real-time nucleic acid sequence-based amplification for RNA detection and amplification, *Anal. Methods*, *3*, 2127–2133, doi:10.1039/c1ay05164d.

Uitz, J., H. Claustre, A. Morel, and S. B. Hooker (2006), Vertical distribution of phytoplankton communities in open ocean: An assessment based on surface chlorophyll, *J. Geophys. Res.*, *111*, C08005, doi:10.1029/2005JC003207.

Uitz, J., H. Claustre, B. Gentili, and D. Stramski (2010), Phytoplankton class-specific primary production in the world's oceans: Seasonal and interannual variability from satellite observations, *Global Biogeochem. Cycles*, *24*, GB3016, doi:10.1029/2009GB003680.

Uz, B., et al. (2001), Pumping of nutrients to ocean surface waters by the action of propagating planetary waves, *Nature*, *409*, 597–600, doi:10.1038/35054527.

Williams, R. G., and M. J. Follows (1998), The Ekman transfer of nutrients and maintenance of new production over the North Atlantic, *Deep Sea Res., Part I*, *45*, 461–489, doi:10.1016/S0967-0637(97)00094-0.

Williams, R. G., and M. J. Follows (2003), Physical transport of nutrients and the maintenance of biological production, in *Ocean Biogeochemistry: The Role of the Ocean Carbon Cycle in Global Change*, edited by M. Fasham, pp. 19–51, Springer, Berlin.

Yentsch, C. S., and D. A. Phinney (1989), A bridge between ocean optics and microbial ecology, *Limnol. Oceanogr.*, *34*, 1694–1705, doi:10.4319/lo.1989.34.8.1694.